Journal of Instrumentation

Development of scanning X-ray fluorescence microscope using KB mirror and white synchrotron radiation at SAGA Light Source

To cite this article: A. Yoneyama and M. Kawamoto 2020 *JINST* **15** P12029

Published by IOP Publishing for Sissa Medialab

Received: *September 1, 2020*
Revised: *September 29, 2020*
Accepted: *November 2, 2020*
Published: *December 22, 2020*

2020 JINST 15 P12029

Development of scanning X-ray fluorescence microscope using KB mirror and white synchrotron radiation at SAGA Light Source

A. Yoneyama[1] **and M. Kawamoto**

SAGA Light Source,
8-7 Yayoigaoka, Tosu, Saga 841-0005, Japan

E-mail: yoneyama@saga-ls.jp

Abstract: A scanning X-ray fluorescence microscope that uses a Kirkpatrick-Baez (KB) mirror and white synchrotron radiation (SR) was developed for obtaining detailed elemental maps within a micro-meter order. The KB mirror is a total reflection mirror, and the white X-rays are focused at a focus point without chromatic aberration. Therefore, the proposed microscope can use strong white and/or pink SR and enable elemental mapping within a practical measurement time at small synchrotron facilities. A feasibility study on the developed microscope was performed by using white SR at the SAGA Light Source in Tosu, Japan. By using the developed microscope, an X-ray microbeam 1 μm in diameter was successfully formed, and a fine elemental map of a Cu mesh and a seed of eustoma were obtained.

Keywords: X-ray fluorescence (XRF) systems; X-ray transport and focusing

[1]Corresponding author.

https://doi.org/10.1088/1748-0221/15/12/P12029

Contents

1 Introduction

The physical and chemical properties of materials depend mainly on the elements, composition ratios, and spatial distribution in samples. The scanning X-ray fluorescence microscope is a powerful tool for fine elemental mapping, and many biomedical [1], material [2], plant [3], fossil [4], art [5], and industrial samples [6] have been observed. However, to use scanning X-ray fluorescence microscopes, highly brilliant X-rays such as synchrotron radiation (SR) at third-generation synchrotron facilities is required, and a long measurement period is required to perform fine observations at small synchrotron facilities such as the SAGA Light Source in Tosu, Japan.

Both a Fresnel zone plate (FZP) [7] and a Kirkpatrick-Baez (KB) [8] mirror are mainly used as X-ray focusing devices in hard X-ray regions. The advantages of the KB mirror are its high reflective efficiently, long working distance (from mirror to sample), and a focal length independent from the wavelength (no chromatic aberration). Moreover, these advantages enable elemental mapping of frozen cells combined with a cryo chamber requiring large space around the sample and micro-two-dimensional X-ray absorption fine structure (micro-2D-XAFS) requiring X-ray energy scanning. Another way of taking advantage of the lack of chromatic aberration is to focus the X-ray of any energy at one point, so high flux white and/or pink SR can be used for microscopic observation [9]. Therefore, a microscope combined with a KB mirror and white (non-monochromated) SR could enable fine elemental mapping (micro-X-ray fluorescence) within a practical measurement period even at a small synchrotron facility.

We report on the development of a scanning X-ray fluorescence microscope system using a KB mirror, the results of a focusing test, and demonstrative elemental observations of a copper mesh and a seed of eustoma grandiflorum using white SR at the SAGA Light Source.

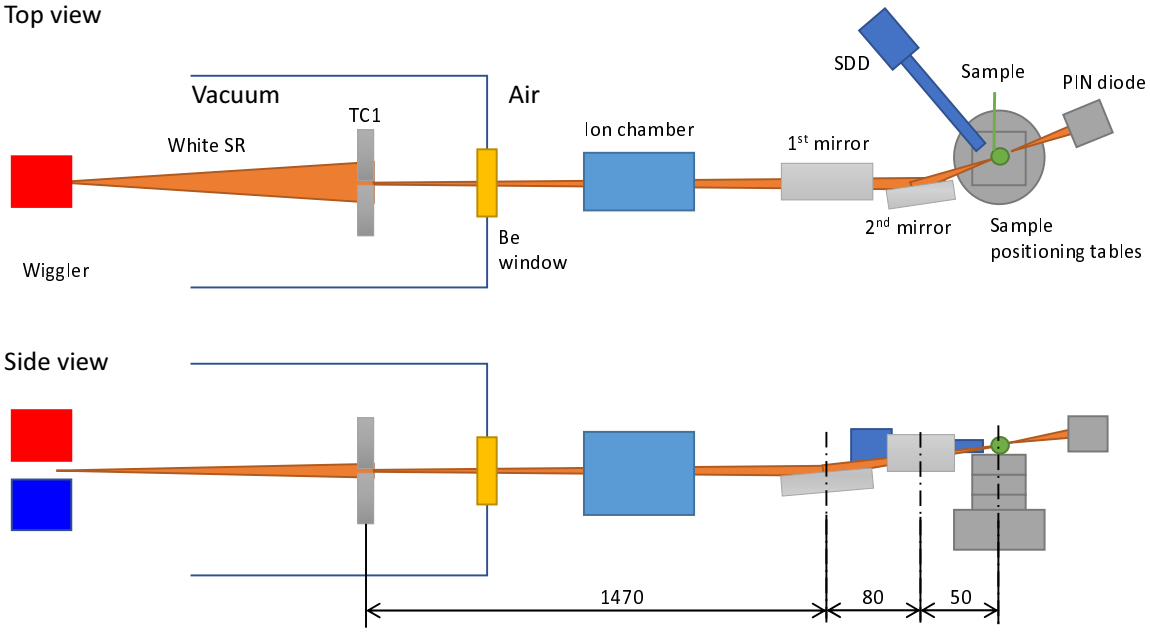

Figure 1. Schematic view of developed microscope using KB mirror at BL07 of SAGA Light Source. White SR emitted from wiggler was inputted to KB mirror directly to keep X-ray intensity high.

2 Scanning x-ray fluorescence microscope

Figure 1 shows a schematic view of a developed hard X-ray microscope system at the beamline 07 (BL07) of the SAGA Light Source. The system is composed of a 4-dimensional X-ray slit (TC1), a KB mirror and its positioning tables, sample positioning tables, a PIN photo diode, and a silicon-drift detector (SDD). The white SR emitted from a super-conducting wiggler of the beamline is cut and formed by the TC1 to be tens of μm^2 as a virtual X-ray source, passed through an ion chamber, and inputted to the KB mirror. Focused X-rays passing through samples are detected by the PIN photo diode. X-ray fluorescence emitted from samples is detected by the SDD with a thin Be window, which is positioned upstream of the samples. The thickness of the Be windows was 100 µm and the spacing between the Be windows and the first mirror was about 500 mm.

Table 1 shows the main specifications of the KB mirror, which was manufactured by JTEC Corporation. The working distance between the downstream end of the second mirror and the focal point was 25 mm, so large samples could be set. The magnifications of the mirror are 1/11.3 and 1/31 for the vertical and horizontal directions, respectively, and the minimum focused beam size was mainly limited by the height and width of the virtual X-ray source (TC1). The surface of the mirrors was coated with 50 nm thick Rh, and the designed incident angle was 10 mrad in both directions, so the calculated cut-off energy was about 7 keV.

Positioning accuracy and stability of micro-m and rad order of the KB mirrors were required for forming a micro X-ray beam, so we designed and developed a new positioning system for the mirror as shown in figure 2. The system consisted of the first unit for precisely positioning the first mirror (M1) (indicated by blue parts in figure 2(a)), the second unit for precisely positioning the second mirror (M2) (indicated by orange parts in figure 2(a)), and a base unit carrying the first and second units. The first unit has a $\theta 1$ table for adjusting the incident angle of M1 against white SR, a

2020 JINST 15 P12029

Table 1. Main specifications of KB mirror.

	First mirror	Second mirror
Size ($L \times W \times T$)	$100 \times 20 \times 10\,\mathrm{mm}^3$	$50 \times 20 \times 10\,\mathrm{mm}^3$
Incident angle	10 mrad	10 mrad
Focal length (source-center)	1470 mm	1550 mm
Focal length (center-focus point)	130 mm	50 mm
Ellipse's major axis length	800 mm	800 mm
Ellipse's minor axis length	4.3714 mm	4.3714 mm
Magnification	1/11.3	1/31
Coating	Rh, 50 nm	Rh, 50 nm
Figure error	2.6 nm	5.6 nm
Roughness	0.176 nm	0.124 nm

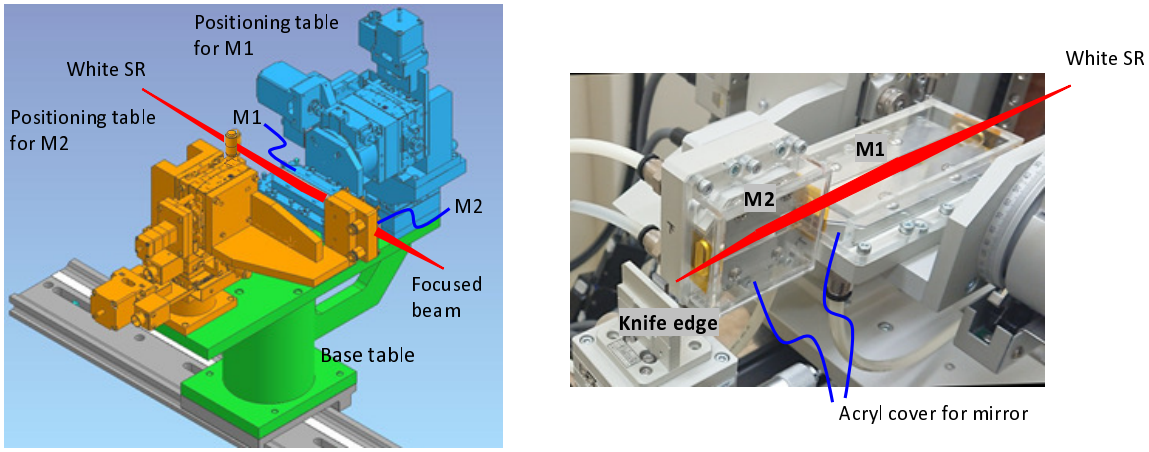

Figure 2. Computer-aided design (CAD) model (a) and photograph (b) of positioning system for KB mirror. Each mirror was positioned by precise positional tables and covered by acrylic case filled with helium gas for decreasing radiation damage.

$\rho 1$ table for adjusting the pitch angle of M1, and a Z1 table for adjusting the vertical position of M1. The second unit has a $\theta 2$ table for adjusting the incident angle of M2 and an X2 table for adjusting the horizontal position of M2. Each table was driven by a stepping motor and controlled remotely by a motor controller (Tsuji Electronics, PM16C-04XDL) from outside of the experimental hatch (radiation shield room covered by Fe plate of 7-mm-thickness). The base unit is loaded on an optical rail laying on an optical bench, and the distance between the TC1 and the positioning system can be adjusted easily by sliding the base unit along the optical path. Each mirror was attached to the positioning table using holders and covered by an acrylic case filled with helium gas for decreasing radiation damage.

The sample positioner was composed of three-axis linear tables (X, Y, and Z axes) and a rotational table. All tables were driven by a stepping motor, and positioning was controlled remotely the same as the positioning system of the mirror. The minimum increment of the linear tables was

2020 JINST 15 P12029

0.05 µm, which was high enough to perform fine elemental mapping. The sample positioner was also loaded on the optical rail, and the coarse working distance between the mirror and sample could be adjusted easily by sliding the sample positioner along the optical path.

3 Results of focusing test and elemental mapping

3.1 Measurement of spectrum of white SR

The energy spectrum of white SR at the BL07 of SAGA Light Source was measured using Si (220) X-ray diffraction of a Si single crystal. White SR emitted from the super-conducting wiggler was cut to form a beam of 0.3×3 mm ($H \times V$) by TC1 and irradiated to the Si crystal positioned on a rotational table of a diffractometer. The diffracted X-ray was detected by an ion chamber loaded on a 2θ-arm of the diffractometer as shown in figure 3. An asymmetric Si crystal (2 degrees) was used to decrease the effect of the scattered X-ray by making the incident angle different from the outgoing angles. In addition, a 3-mm-wide X-ray slit was set in front of the ion chamber to decrease the effect of the scatted X-ray. Mixed gas composed of nitrogen (85%) and argon (15%) gas that was robust to the high-energy X-ray was used to suppress the contamination of the higher-order X-ray diffraction such as Si (440).

Figure 4 shows the X-ray spectrum obtained by a step scanning measurement of $\theta - 2\theta$ (moving the θ table and the 2θ arm simultaneously; blue line), the calculated reflectivity of the KB mirror (M1 and M2; orange line) [10], and the calculated X-ray spectrum after reflection of the KB mirror (spectrum of incident X-ray to sample; green line). The scanning range of the θ table was 2 to 37 degrees corresponding to 92.34 ~ 5.65 keV and step width was 0.25 degrees. Although the calculated peak energy of the emitted white SR from the wiggler was 7 keV [11], the obtained peak energy was about 14 keV because of the absorption of the lower energy X-ray by the air and Be window. On the other hand, the reflectivity of the X-ray above 10 keV was very small, and therefore the peak energy of the refracted X-ray was shifted to 6.5 keV and the full width at half maximum (FWHM) of the peak was sharpened to 2 keV.

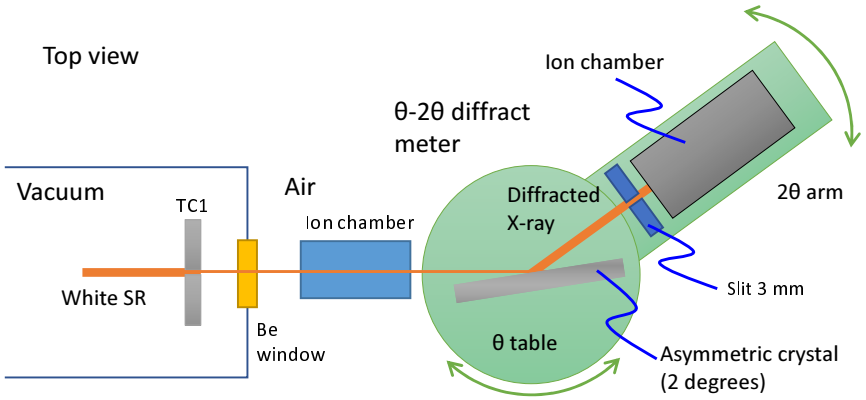

Figure 3. Schematic view of X-ray diffraction measurement for white SR spectrum. X-ray diffraction of Si (220) of asymmetric crystal was used to decrease the effect of scattered X-ray.

2020 JINST 15 P12029

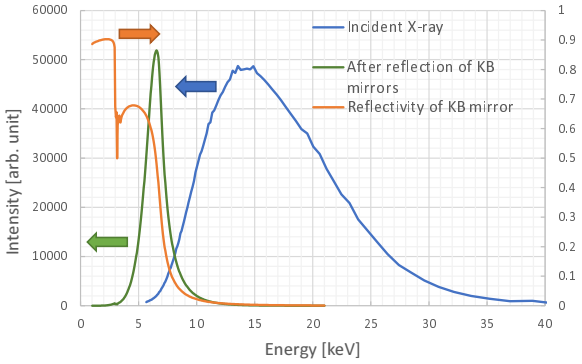

Figure 4. Obtained X-ray spectrum of white SR (blue), calculated reflectivity of KB mirror (M1 and M2; orange), and calculated X-ray spectrum (green) after reflection of KB mirror.

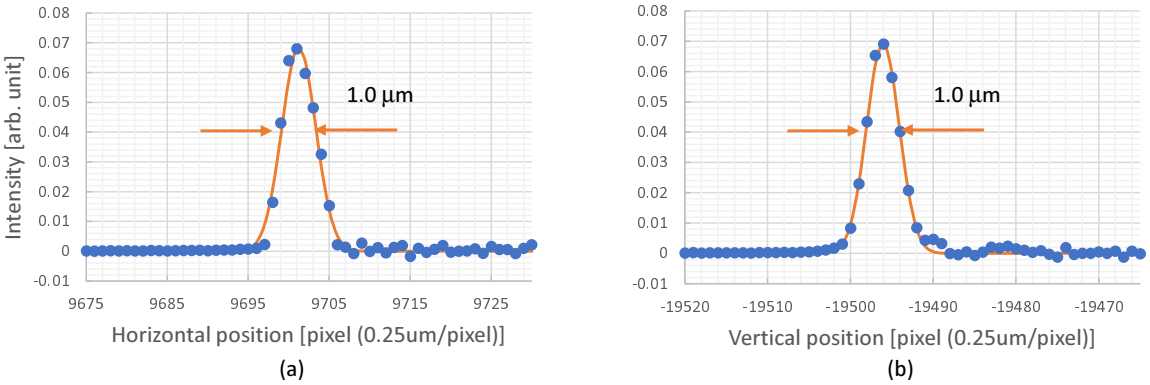

Figure 5. Beam profile of focused white SR X-ray beam in horizontal (a) and vertical (b) directions. Profiles of 1 µm in both directions were obtained by using knife-edge scanning method.

3.2 Results of focusing test

A beam profile of the focused white SR X-ray beam was measured by using a knife-edge scanning method with a Pb knife edge placed at the focus point. Figure 5 shows the obtained beam profile for the vertical (a) and horizontal (b) directions. The knife edge was scanned in 0.25-µm steps, and the intensity was detected by the PIN diode with a 0.5-s exposure. The results show that the X-ray beam was focused 1.0 µm in both directions without any sub-peak. The width and height of the TC1 were set at 20 and 10 µm, respectively. The measured beam size of the vertical direction well coincided with the ideal beam size. On the other hand, the horizontal beam size was wider than the ideal size because the distance between the TC1 and M2 differs from the ideal distance. The TC1 was composed of independent vertical and horizontal water cooled slits 40 mm set apart, and therefore the distance between TC1 and M1 could be set as the ideal value whereas the distance between the TC1 and M2 could not be kept the ideal value.

3.3 Results of elemental mapping

An elemental mapping of a copper mesh (1500 line-space/inch, the bar width was 5 µm and the hole width was 11.5 µm) by using the on-the-fly-scanning method [12] (moving the sample positioning table on the x-axis and detecting transmitted and fluorescent X-rays continually) was performed for

2020 JINST 15 P12029

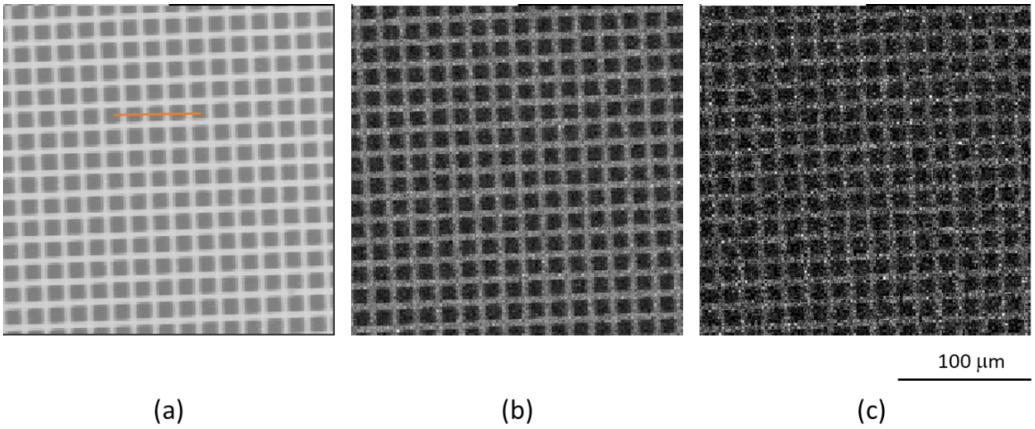

Figure 6. (a) Transmitted and (b) fluorescent Cu K_α and (c) Cu K_β images of Cu mesh (1500 LS/inch) obtained with on-the-fly-scanning method. Total measurement period was 2400 s, and exposure time was 50 ms/point.

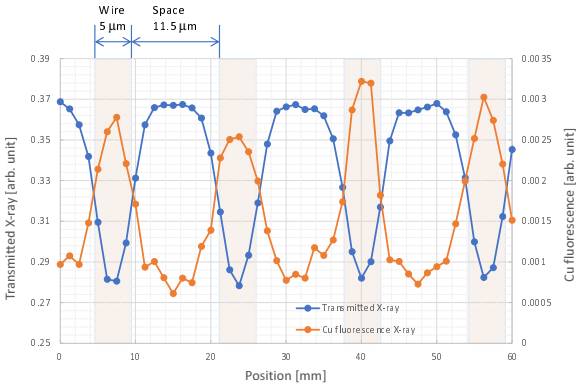

Figure 7. Line profiles of transmitted X-ray and fluorescence X-ray intensities of orange line in figure 6(a).

a feasibility test of the developed microscope. The transmitted and fluorescent X-rays were detected by a Si-PIN photo diode (OKEN S-2500) and SDD (AMPTEK XR100SDD with C1 window (silicon nitride (Si3N4) with an aluminum coating)), respectively, as shown in figure 1. Figure 6 shows obtained (a) transmitted and (b) fluorescent Cu K_α and (c) Cu K_β images. The image was $250 \times 250\,\mu m^2$, and the number of points was 200×200 (step width was 1.25 µm). The total measurement period was 2400 s, and the exposure time was 50 ms/point. Fine and detailed images were obtained owing to the 1-µm focused beam and strong white SR despite the short exposure time.

Figure 7 shows the line profiles of transmitted X-ray and the fluorescence X-ray (sum of Cu K_α and K_β) intensity of the orange line in figure 6. The results showed that the width of the Cu wire edge is about 2 pixels, and therefore the spatial resolution was estimated to be about 2.5 µm because the pixel size (step width) in this measurement was 1.25 µm. The low resolution compared to the beam profile (1 µm) in figure 5 was mainly due to the effect of the widespread in the base of the focused X-ray beam and the signal averaging by the on-the-fly-scanning method.

As the next step, elemental mapping of Eustoma (eustoma grandiflorum) seeds was performed using the same experimental setup. The seeds were fixed on double-sided tape, and the tape was

2020 JINST 15 P12029

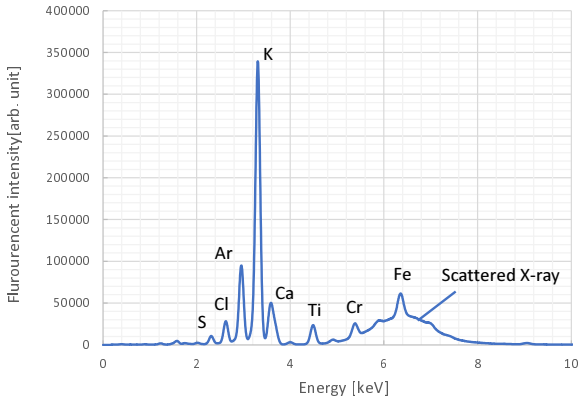

Figure 8. Obtained fluorescence X-ray spectrum. Many elements such as S, Cl, K, Ca, and Fe were contained in seeds. Broad peak near 6.5-keV was assumed to be caused by elastic (Rayleigh) and inelastic (Compton) scattering because the spectrum is a similar shape to the incident X-ray (figure 4, green line).

attached to the tip of a thin needle. The scanning area was $750 \times 625\,\mu m^2$, and the number of points was 600×500 (step width was 1.25 µm). The total measurement period was 8650 s, and the exposure time was 25 ms/point.

Figure 8 shows an obtained fluorescence X-ray spectrum of a seed during the whole measurement. Spectrum peaks could be detected at 2.3, 2.6, 3.0, 3.3, 3.6, 4.5, 5.4, and 6.4-keV corresponding to S, Cl, Ar, K, Ca, Ti, Cr, and Fe fluorescent X-rays. The seeds were placed in the air, so the Ar in the air was detected. In addition, spatial distributions of Ti and Cr formed a uniform intensity, so both signals came from the sample and mirror positioner. Consequently, S, Cl, K, Ca, and Fe were assumed to be contained in the seeds. A broad peak from 5 to 7.5 keV was assumed to be caused by elastic (Rayleigh) and inelastic (Compton) scattering because the spectrum is a similar shape to the incident X-ray (figure 4, green line). Note that the X-ray intensity above 8 keV was cut by reflection of the KB mirror, and therefore K-fluorescence X-ray of elements heavier than Ni (its K-absorption edge is at 8.33 keV) and L-fluorescence X-ray of elements heavier than Ho (its L-III edge is at 8.07 keV) could not be detected.

Figure 9 shows an obtained transmitted image and obtained fluorescent S, Cl, K, and Ca images. In this measurement, we first determined the elements to be measured (such as S, Cl, K, and Ca), set the ROI on the spectrum, and only detected the signal counts of each ROI, because long transferring period was required for measuring the entire spectrum. Therefore, the signal included fluorescence X-rays and scattered X-rays for all elements. The transmitted image (left) shows that the surface of the seed was covered with many uneven structures. The fluorescent K image also shows a similar structure, and therefore the K element was thought to be distributed near the surface of the seed, which coincides with the distribution of rice [13, 14]. In addition, small high concentrated spots of S and Cl elements were observed near the bottom-right region in the seed shown as an orange circle, and therefore the region was assumed to be a germ and the other region an endosperm [15, 16].

4 Discussion

The X-ray photon flux in front of the KB mirror was estimated at 6×10^9 photons/s from the ionization current of the ion chamber, and therefore the X-ray flux at the sample position was

2020 JINST 15 P12029

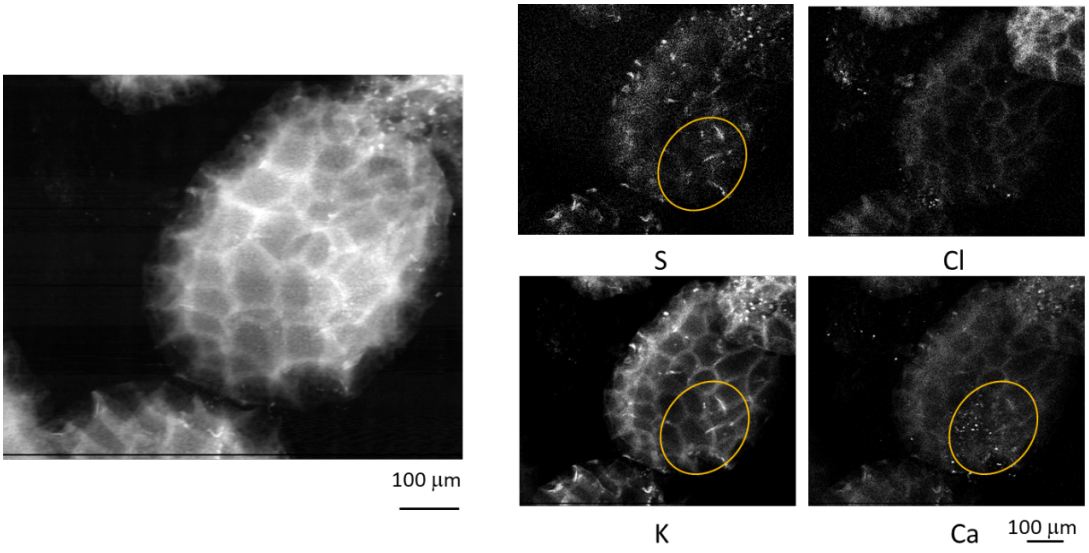

Figure 9. Transmitted (left) and fluorescent S, Cl, K, and Ca images of eustoma grandiflorum seeds. The scanning area was $750 \times 625\,\mu m^2$, and the total measurement period was 8650 s.

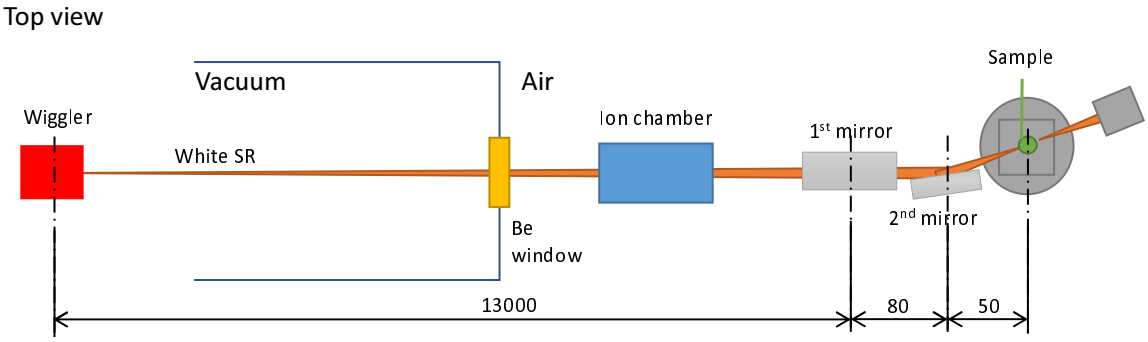

Figure 10. Schematic view of optical configuration of microscopy using SR light source of wiggler as X-ray source of KB mirror. No X-ray slit is required, and strong X-ray photon flux can be obtained.

calculated at 4×10^7 photons/s using the reflectivity of the KB mirror. The big mismatch between the spectrum of the incident X-ray and the reflectivity of the KB mirror shown in figure 4 causes significantly reduced X-ray photon flux, and the flux was decreased to about 1/200 of that of a microbeam system at SPring-8 [17]. In other words, a KB mirror that has a cut-off energy above 10 keV (the incident angle was smaller than 5 mrad) enables the high X-ray flux to be kept at the 10^9 photons/s order, and transmitted and fluorescent X-ray images are expected to be finely observed within practical measurement periods. In addition, high-energy X-ray photon flux above 10-keV is increased dramatically, and fine mapping of metallic elements is also expected to be possible.

The beam size in front of the TC1 slit was 4×0.4 mm ($H \times V$), which is much larger than the width and height of the TC1 ($20 \times 10\,\mu m$) to form a focused 1-µm X-ray beam, so the X-ray photon flux of 1/8000 of the incident X-ray was used for observations. To overcome this limitation, a new optical configuration is currently under consideration that uses the SR light source of the wiggler as the X-ray source of the KB mirror as shown in figure 10. The configuration does not require any optical

2020 JINST 15 P12029

components such as an X-ray slit between the source and the mirror, and therefore about 625 times stronger X-ray photon flux is expected, even taking into account the small acceptance (0.5×0.25 mm) of the KB mirror. On the other hand, radiation damage of samples is unavoidable in X-ray microscopy, so two observation modes are planned by using a deformable KB mirror [18]: fast but hard radiation damage (configuration in figure 10) and slow but soft damage (configuration in figure 1).

5 Conclusion

A scanning fluorescence X-ray microscope that uses a Kirkpatrick-Baez (KB) mirror was developed and tested by using white synchrotron radiation (SR) at the SAGA Light Source in Tosu, Japan. The width and height of the focused X-ray beam were 1 μm in both directions in a focusing test done using the knife-edge scanning method. Fine and detailed transmitted and fluorescent images of a Cu mesh and an eustoma seed were obtained by the on-the-fly-scanning method. These results show that the developed microscope can perform fine elemental mapping within a practical measurement period by using white SR. For the next step, we are planning to perform a feasibility study on a full-field X-ray microscope with the developed system and introduce a new KB mirror whose cut-off energy is above 10 keV to reduce the intensity loss caused by reflection of the KB mirror.

Acknowledgments

We would like to express our appreciation to Mr. Kenichirou Sakamoto and Ms. Akane Matsumoto of the Agricultural Research Center of Saga Prefecture for preparing the eustoma grandiflorum seeds. The study was carried out under the approval (proposal no. 190202I) of the Committee of the SAGA Light Source.

References

[1] S. Matsuyama, K. Maeshima and M. Shimura, *Development of x-ray imaging of intracellular elements and structure*, *Journal of Analytical Atomic Spectrometry* **35** (2020) 1279.

[2] G. Martínez-Criado, *Application of Micro- and Nanobeams for Materials Science*, in E. Jaeschke et al. eds., *Synchrotron Light Sources and Free-Electron Lasers: Accelerator Physics, Instrumentation and Science Applications*, Springer, Cham (2016), pp. 1505–1539.

[3] P.M. Kopittke, T. Punshon, D.J. Paterson, R.V. Tappero, P. Wang, F.P.C. Blamey et al., *Synchrotron-based x-ray fluorescence microscopy as a technique for imaging of elements in plants*, *Plant Physiol.* **178** (2018) 507.

[4] U. Bergmann, L. Bertrand, N.P. Edwards, P.L. Manning and R.A. Wogelius, *Chemical Mapping of Ancient Artifacts and Fossils with X-Ray Spectroscopy*, in E. Jaeschke et al. eds., *Synchrotron Light Sources and Free-Electron Lasers: Accelerator Physics, Instrumentation and Science Applications*, Springer, Cham (2020), pp. 2393–2455.

[5] L.M. Smieska, A.R. Woll, F. Vanmeert and K. Janssens, *Synchrotron-based high-energy x-ray MA-XRF and MA-XRD for art and archaeology*, *Synchrotron Radiat. News* **32** (2019) 29.

[6] F. Lin etv al., *Synchrotron X-ray Analytical Techniques for Studying Materials Electrochemistry in Rechargeable Batteries*, *Chemical Reviews* **117** (20178) 13123.

2020 JINST 15 P12029

[7] G. Schmahl, D. Rudolph, B. Niemann and O. Christ, *Zone-plate x-ray microscopy*, *Quart. Rev. Biophys.* **13** (1980) 297.

[8] P. Kirkpatrick and A.V. Baez, *Formation of optical images by x-rays*, *J. Opt. Soc. Am.* **38** (1948) 766.

[9] N. Tamura, A.A. MacDowell, R. Spolenak, B.C. Valek, J.C. Bravman, W.L. Brown et al., *Scanning x-ray microdiffraction with submicrometer white beam for strain/stress and orientation mapping in thin films*, *J. Synchrotron Radiat.* **10** (2003) 137.

[10] B. Henke, E. Gullikson and J. Davis, *X-ray interactions: Photoabsorption, scattering, transmission, and reflection at e = 50-30,000 eV, z = 1-92*, *Atomic Data and Nuclear Data Tables* **54** (1993) 181.

[11] M. Kawamoto, K. Sumitani and T. Okajima, *The design of superconducting wiggler beamline BL7 at SAGA-LS*, *AIP Conf. Proc.* **1234** (2010) 355.

[12] I. McNulty, S.P. Frigo, C.C. Retsch, Y. Wang, Y. Feng, Y. Qian et al., *Design and performance of the 2-ID-B scanning X-ray microscope*, *Proc. SPIE* **3449** (1998) 67.

[13] T. Iwai, M. Takahashi, K. Oda, Y. Terada and K.T. Yoshida, *Dynamic changes in the distribution of minerals in relation to phytic acid accumulation during rice seed development*, *Plant Physiol.* **160** (2012) 2007.

[14] T. Punshon, K. Hirschi, J. Yang, A. Lanzirotti, B. Lai and M.L. Guerinot, *The role of CAX1 and CAX3 in elemental distribution and abundance in arabidopsis seed*, *Plant Physiol.* **158** (2011) 352.

[15] L. Lu, S. Tian, H. Liao, J. Zhang, X. Yang, J.M. Labavitch et al., *Analysis of metal element distributions in rice (oryza sativa l.) seeds and relocation during germination based on x-ray fluorescence imaging of zn, fe, k, ca, and mn*, *PLoS ONE* **8** (2013) e57360.

[16] B. Meng, X. Feng, G. Qiu, C.W.N. Anderson, J. Wang and L. Zhao, *Localization and speciation of mercury in brown rice with implications for pan-asian public health*, *Environ. Sci. Technol.* **48** (2014) 7974.

[17] Y. Hirai, S. Yasuami, A. Kobayashi, Y. Hirai, J. Nishino, M. Shibata et al., *The design and performance of beamline BL16xu at SPring-8*, *Nucl. Instrum. Meth. A* **521** (2004) 538.

[18] S. Matsuyama, H. Nakamori, T. Goto, T. Kimura, K.P. Khakurel, Y. Kohmura et al., *Nearly diffraction-limited x-ray focusing with variable-numerical-aperture focusing optical system based on four deformable mirrors*, *Sci. Rep.* **6** (2016) 24801.

2020 JINST 15 P12029